Paper IV

Phases of the SAW reflection and transmission coefficients for short reflectors on 128° LiNbO3

S. Lehtonen, V. P. Plessky,
N. Béreux, and M. M. Salomaa

IV

Phases of the SAW reflection and transmission coefficients for short reflectors on 128° $LiNbO_3$

Saku Lehtonen, Victor P. Plessky, *Senior Member, IEEE*, Natacha Béreux, and Martti M. Salomaa, *Member, IEEE*

Abstract

We study numerically the phase of surface acoustic waves reflected by or transmitted through short reflectors comprising only 1–3 aluminium electrodes on 128° YX-cut $LiNbO_3$. The electrodes have a finite thickness and they are either open-circuited or grounded. The center-to-center distance between adjacent electrodes d corresponds roughly either to half of the characteristic wavelength $d \propto \lambda_0/2$ or to $d \propto \lambda_0$, for the reflectors operating at the fundamental and second harmonic modes, respectively. We use software based on the finite-element and boundary-element methods (FEM/BEM) for numerical experiments with a tailored 3-IDT test structure, simulating experimental conditions with an incident wave and reflected and transmitted SAWs. Employing artificial enhancement of time resolution in conjunction with the fast Fourier transform (FFT) and time-gating, calculation of the Y-parameters in a relatively wide frequency range allows us to determine the phase of the reflection and transmission coefficients.

I. Introduction

In this paper, we report the third part of the simulated results for reflectors comprising 1-3 electrodes. Here, we concentrate on the phases of the reflection and transmission coefficients. The magnitude of the former as well as quantitative estimates of attenuation due to scattering into the bulk were reported in Ref. [1]. The optimum electrode geometry was considered in Ref. [2].

We continue the study of short reflectors (different thicknesses of the aluminium electrodes and metallization ratios are considered) operating both at the fundamental frequency, when the center-to-center distance between the adjacent fingers d is comeasurable with half the SAW wavelength $\lambda_0/2$ or, at the 2nd harmonic, with d close to λ_0.

S. Lehtonen (e-mail: saku@focus.hut.fi) and M. M. Salomaa (e-mail: Martti.Salomaa@hut.fi) are with the Materials Physics Laboratory, Helsinki University of Technology, P.O. Box 2200, FIN-02015 HUT, Finland.

V. P. Plessky is with GVR Trade SA, Rue du Château 9 C, CH-2022 Bevaix, Switzerland (e-mail: victor.plessky@bluewin.ch).

N. Béreux is with Centre de Mathématiques Appliquées, UMR 7641 CNRS/Ecole Polytechnique, 91228 Palaiseau cedex, France (e-mail: natacha@cmapx.polytechnique.fr).

Conservation of energy implies that the reflection and transmission coefficients are in phase quadrature ±90° [3]. The same result is obtained from the equivalent circuit model by analysis of wave reflection from small impedance discontinuities [4]. Often, the reflection coefficient of a single electrode is defined by $R = -jR_0$ [5]. For most materials, R_0 is a real positive value but, for the particular case of either open-circuited electrodes or shorted electrodes with rather heavy mass loading on 128° $LiNbO_3$, R_0 has a negative sign and the phase is about +90° [5]. To avoid any ambiguity, we will always refer to the total reflection coefficient $R = |R|e^{j\cdot \mathrm{Phase}\cdot 180/\pi}$.

In a rough approximation, the Rayleigh-wave reflection from a single electrode corresponds to the one-dimensional problem of reflection of a bulk wave from a layer of an acoustically different medium. The solution of this classical problem is straightforward. For reference, the formulas for the reflection and transmission coefficients are reproduced here for arbitrary elastic media. No assumption is implied that the difference in acoustic properties of the two media is small.

Consider an isotropic medium constrained by two semi-infinite layers of another isotropic medium and a longitudinal bulk wave propagating towards the positive x-direction $\vec{u} = (u_x, 0, 0)$, incident on the first boundary, see Fig. 1. Introducing the trial solutions for the incident, reflected and transmitted waves with the reference point at x = 0,

$$\text{Zone I:} \quad u_{\mathrm{I}} = u_0 e^{-i(k_1 x - \omega t)} + u_R e^{i(k_1 x + \omega t)}, \tag{1}$$

$$\text{Zone II:} \quad u_{\mathrm{II}} = u_1 e^{-i(k_2 x - \omega t)} + u_2 e^{i(k_2 x + \omega t)}, \tag{2}$$

$$\text{Zone III:} \quad u_{\mathrm{III}} = u_T e^{-i(k_1 x - \omega t)}, \tag{3}$$

one can calculate the stress and strain fields. Applying Newton's law and the boundary conditions that both the deformation and stress be continuous

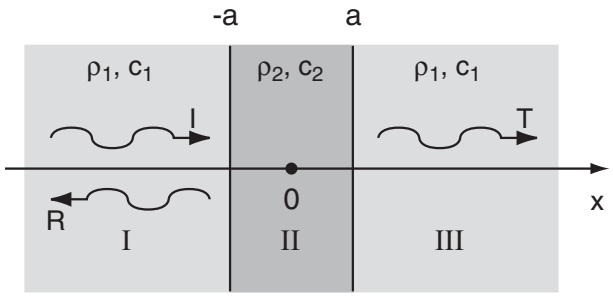

Fig. 1. Schematic of the one-dimensional purely mechanical scattering problem.

across the boundaries at $x = -a$ and $x = a$ one arrives at the expressions for the amplitude reflection and transmission coefficients:

$$R = -i\frac{2\left(1-\sqrt{\frac{\rho_1 c_1}{\rho_2 c_2}}^2\right)\sin(2k_2 a)e^{2i(k_1-k_2)a}}{\left(1+\sqrt{\frac{\rho_1 c_1}{\rho_2 c_2}}\right)^2-\left(1-\sqrt{\frac{\rho_1 c_1}{\rho_2 c_2}}\right)^2 e^{-4ik_2 a}}, \quad (4)$$

$$T = \frac{4\sqrt{\frac{\rho_1 c_1}{\rho_2 c_2}}e^{2i(k_1-k_2)a}}{\left(1+\sqrt{\frac{\rho_1 c_1}{\rho_2 c_2}}\right)^2-\left(1-\sqrt{\frac{\rho_1 c_1}{\rho_2 c_2}}\right)^2 e^{-4ik_2 a}}, \quad (5)$$

where ρ_i, c_i and k_i are the density, stiffness and wave vector in the medium $i = 1, 2$. Note that for arbitrary parameters for the two media, the phase difference given by R/T is seen to be $\pm 90°$. However, the phase of the reflection coefficient is not necessarily exactly equal to $\pm 90°$ because of the two exponential factors in Eq. (4). The exponential term in the numerator corresponds to the delays inside the middle layer while the one in the denominator can be attributed to multiple reflections. The same effects accordingly shift the phase of the transmission coefficient.

Figure 2(a) displays the phase of the reflection coefficient for the case where the middle layer has a lower acoustic impedance than the semi-infinite layer I and III (see Fig. 1), its width being either a quarter of or half a wavelength in medium II. The former corresponds to the fundamental-mode electrode with $a = \lambda_0/4$ and the latter to an electrode operating at the second harmonic frequency with $a = \lambda_0/2$. It can be seen that for the $\lambda_0/4$ case, the phase of the reflection coefficient is close but not exactly equal to $+90°$. For the simulated $\lambda_0/2$ case, the phase changes sign at some frequency where the reflection coefficient of Eq. (4) passes through zero. If the layer in the middle were acoustically denser,

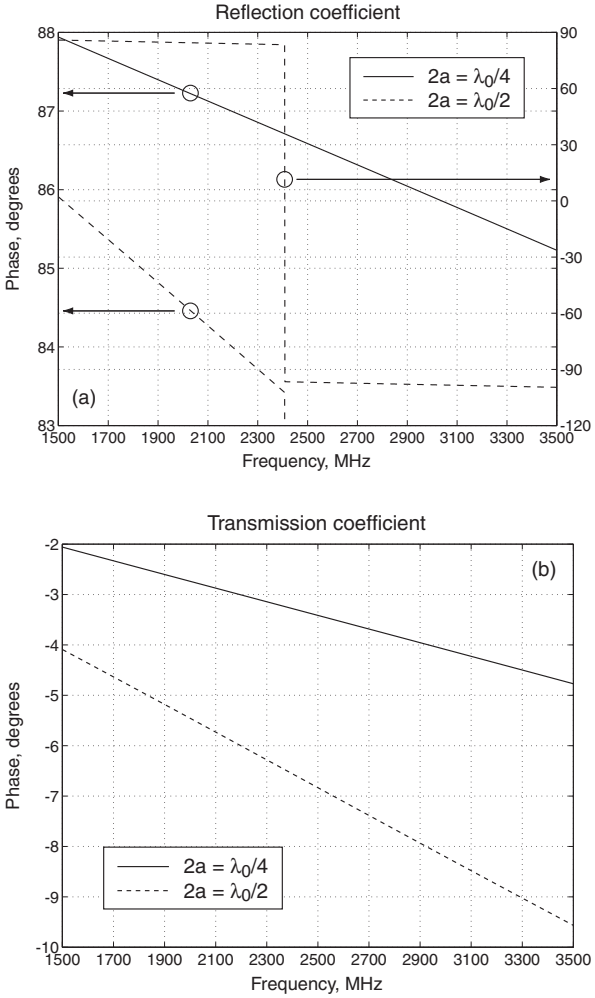

Fig. 2. Theoretically calculated phases of the reflection and transmission coefficients in the problem of Fig. 1. Solid line: $\lambda_0/4$-wide middle layer. Dashed line: $\lambda_0/2$-wide middle layer. (a): Reflection coefficient. (b): Transmission coefficient.

the reflection coefficient would have an opposite sign with its phase close to –90°.

Figure 2(b) displays the phase of the transmission coefficient for the corresponding geometries; it is not exactly zero reflecting the fact that the wave is delayed inside the middle layer, and the delay increases with frequency.

II. Simulation methods

In this paper, we further analyze the simulation results obtained earlier for short reflectors on 128° $LiNbO_3$ [1]. The calculations were carried out using a rigorous simulation tool [6, 7] which describes the substrate via Green's functions, uses the finite-element method (FEM) to compute the fields on the electrodes and combines the two regimes by the

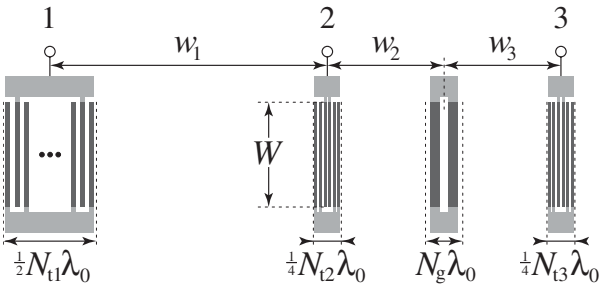

Fig. 3. Test structure for simulations of short reflectors on 128° $LiNbO_3$. The values $N_{t1} = 21$, $N_{t2} = N_{t3} = 6$, $N_g = 1 \ldots 3$, $\lambda_0 = 1.6$ μm, $W = 200$ μm, $w_1 = 160$ μm, and $w_2 = w_3 = 64$ μm are used.

boundary-element method (BEM). In the simulations, intrinsic material losses were excluded from Green's functions and the resistivity of the electrodes was ignored.

The test structure used in the numerical experiments, see Fig. 3, includes rather long and efficient an input transducer (electrical port 1), two identical split-finger receiving transducers with only a few electrodes (ports 2 and 3) and the device under test, the reflector, placed between the receiving transducers. A similar structure was used some time ago by P. Wright in experimental measurements of the properties of SAW metallic gratings [8]. As discussed in Ref. [1], the guidelines for selecting the numbers of fingers in the different elements are, on one hand, the aim to minimize the frequency and time dispersion caused by the DUT to the incident signal and, on the other hand, a feasible simulation time. The center-to-center distances between the elements in the test structure were chosen such that the partial signals of interest, registered at ports 2 and 3, have equally long propagation paths and hence, identical propagation times. The wavelength of the input transducer is 1.6 μm ($p = 0.8$ μm) which corresponds to a center frequency close to 2.5 GHz on the 128° $LiNbO_3$ substrate.

To describe the perturbation brought about by the DUT to the incident SAW, we use the fact that the Y-parameters Y_{21} and Y_{31} are actually proportional to the currents generated in the IDTs at ports 2 and 3 and, thus, proportional to the SAW amplitudes incident on the transducers. Moreover, the complex-valued elements of the admittance matrix contain the frequency-dependent phase information attributed to the reflection from and transmission through the DUT of the incident wave. The time-gating procedure described in Ref. [1] allows one to extract from Y_{31} and Y_{21} the contribution of the direct transmitted wave (Y_{31}^{d}) and that of the wave reflected from the grating (Y_{21}^{r}).

Following Ref. [1], the reference signal to which the reflected and transmitted waves are compared is the direct signal registered at port 3, obtained from a simulation of the operation of a test structure *in the absence of the reflector*, $Y_{31}^{\mathrm{d,\,ref}}$. This procedure allows one to exclude the perturbation caused by the split-finger transducer at port 2.

The frequency step Δf and simulation bandwidth B were set to 4 MHz and 2 GHz, thus yielding a 501-point frequency grid. In the time domain, according to

$$T = \frac{1}{\Delta f}, \tag{6}$$

$$\Delta t = \frac{1}{\mathrm{B}}, \tag{7}$$

the total time span T and the interval between time points Δt are 250 ns and 0.5 ns, respectively. The time resolution of the simulation approximately corresponds to the SAW propagation distance of 4000 m/s $\cdot$ 0.5 ns = 2 μm, which is longer than the SAW wavelength at the center frequency (1.6 μm). However, the phase changes attributed to the perturbation caused by the electrodes may be only a fraction of the full cycle. Thus, in order to extract reliable data of the phase of the waves reflected from and transmitted through the short grating, it is necessary to address the problematics of the insufficient time resolution.

To render details of the time responses visible, we use the following procedure. The time resolution is enhanced if the frequency bandwidth is increased, see Eq. (7). We continuously add dummy points to the simulated frequency response, maintaining the adopted frequency spacing $\Delta f = 4$ MHz. As a consequence, the time span is not affected, see Eq. (6). The level of admittance of the dummy points is set close to zero so as not to distort the original response. By adding zeros to the frequency response in the regions where the response is negligible, the simulated response remains physically intact, *i.e.*, no new information is added. In principle, such a wideband response could be calculated with the FEM/BEM software used [6, 7] but, knowing the response to have a negligible amplitude in these frequency ranges, this procedure allows tremendous savings in simulation time. To suppress the influence of the resulting abrupt changes in the level of the extended frequency-domain signal, a weighting function is applied to smoothen the transitions from the low and high-frequency ends of the original frequency response to the minimum level of the

extension bands. For the weighting we use

$$W = 1 - \left(\frac{f - f_c}{\Delta f} \right)^{10}, \tag{8}$$

where

$$f_c = \frac{f_{\mathrm{beg}} + f_{\mathrm{end}}}{2},$$
$$\Delta f = \frac{f_{\mathrm{end}} - f_{\mathrm{beg}}}{2},$$

and f_{beg} and f_{end} denote the lowest and the highest frequency points of the simulated response, respectively. As a result, only the insignificant parts of the frequency response are adjusted, see Fig. 4.

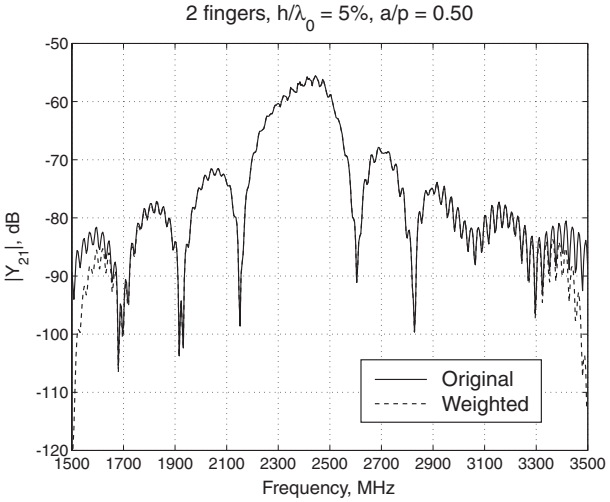

Fig. 4. Illustration of the manipulation of the simulated frequency response to enhance time resolution. Solid line: Original response. Dashed line: Weighted response.

Adding 374 dummy points in the region covering the frequencies 4...1496 MHz and 9125 dummy points covering the frequencies 3504...40000 MHz, we obtain a 10000-point frequency grid with the frequency step $\Delta f = 4$ MHz and an extended bandwidth of $B_{\mathrm{ext}} = 40$ GHz. The resulting time resolution is $B_{\mathrm{ext}}^{-1} = 0.025$ ns, and the corresponding SAW propagation distance is roughly 4000 m/s $\cdot$ 0.025 ns $= 0.1$ μm, only a fraction of the SAW wavelength at the center frequency ($\lambda_0 = 1.6$ μm). The procedure described above thus allows to illustrate the signals in the time domain in the form of sinusoidal waves, instead of only seeing sparsely spaced points of the same sinusoids.

The reflection and the transmission coefficients are obtained through time gating (for details and values, see the first part of this work, Ref. [1]). The phases of the reflected and transmitted signals are evaluated in both the frequency and time domains. In the former, the result is presented in a frequency band about the central frequency, and in the latter, values averaged over a time span corresponding to the interaction of the transmitted pulse with the receiving transducers (reflected pulse at port 2 and reference pulse at port 3) are given.

In the frequency domain, the phase of the reflection coefficient is extracted simply from

$$\angle\left[\mathrm{R_f}\right] = \frac{360^\circ}{2\pi} \cdot \angle\left(\frac{\mathrm{Y}_{21}^{\mathrm{r}}(\mathrm{f})}{\mathrm{Y}_{31}^{\mathrm{d,ref}}(\mathrm{f})} \right), \tag{9}$$

where $\mathrm{Y}_{21}^{\mathrm{r}}$ is the time-gated reflected signal contribution in the frequency-domain, and $\mathrm{Y}_{31}^{\mathrm{d,ref}}$ is the time-gated direct signal observed at port 3 in the absence of the reflector. The phase of the reflection coefficient was also studied in the time domain. Values averaged over the time span Δt corresponding to the interaction of the pulse transmitted form port 1 with the receiving transducers (reflected pulse at port 2 and reference pulse at port 3) are considered. The chosen averaging time span Δt extends from 72.5 to 75 ns, see Figs. 5–6.

$$\angle\left[\mathrm{R_t}\right] = \frac{360^\circ}{2\pi} \cdot \mathrm{mean}\left\{ \angle\left(\frac{\mathrm{Y}_{21}^{\mathrm{r}}(\mathrm{t})}{\mathrm{Y}_{31}^{\mathrm{d,ref}}(\mathrm{t})} \right) \right\}_{\Delta t}. \tag{10}$$

The same guidelines were followed for the extraction of the phase of the transmission coefficient:

$$\angle\left[\mathrm{T_f}\right] = \frac{360^\circ}{2\pi} \cdot \angle\left(\frac{\mathrm{Y}_{31}^{\mathrm{d}}(\mathrm{f})}{\mathrm{Y}_{31}^{\mathrm{d,ref}}(\mathrm{f})} \right), \tag{11}$$

$$\angle\left[\mathrm{T_t}\right] = \frac{360^\circ}{2\pi} \cdot \mathrm{mean}\left\{ \angle\left(\frac{\mathrm{Y}_{31}^{\mathrm{d}}(\mathrm{t})}{\mathrm{Y}_{31}^{\mathrm{d,ref}}(\mathrm{t})} \right) \right\}_{\Delta t}, \tag{12}$$

where the signals $\mathrm{Y}_{31}^{\mathrm{d}}$ and $\mathrm{Y}_{31}^{\mathrm{d,ref}}$ are the admittances observed in the presence and absence of the reflector, respectively. The propagation distances of the transmitted and the reference signals are obviously exactly equal.

III. Pulse representation

The influence of the grating on the incident pulse can be studied by comparing the time responses of the partial signals. In Figs. 5–6, the real part of the time-domain admittance of the reflected signal corresponding to reception at port 2 after reflection from the reflector studied ($\mathrm{Re}\{\mathrm{Y}_{21}^{\mathrm{r}}\}$) is compared to the real part of the reference signal received at port 3 (with no reflector present, $\mathrm{Re}\{\mathrm{Y}_{31}^{\mathrm{d,ref}}\}$). Taking the reflection center to be located in the middle of the reflector, the propagation paths of the signals

are equal. Note that the scales of the responses are different. The metal thickness in each figure is $h/\lambda_0 = 5\%$, and the metallisation ratio is $a/p = 0.5$. The grating length is varied from 1 to 3 electrodes. In Fig. 5, the operation of the fundamental-mode grating is illustrated, and in Fig. 6, the second-harmonic gratings are considered.

It is to be noted that partial reflections from the individual reflector electrodes have different propagation paths. The centers of the electrodes may be shifted with respect to the center of the reflector. For the single-electrode case, the center of the electrode evidently coincides with the center of the reflector. For 2-electrode gratings, however, the center of the reflector is located in the middle of the gap between the grating electrodes, and for 3-electrode gratings, the center of the reflector coincides with the center of the middle electrode. Consequently, for 2- and 3-electrode reflectors, the reflected pulse is slightly wider than the incident pulse in the time domain.

Two effects have an influence on the form of the reflected signal. First, the distributed electrodes give rise to partial reflections, which have different propagation paths, some of which are shorter and some longer than that of the reference signal ($Y_{31}^{d,\,ref}$). In Figs. 5–6, especially for 3 electrodes, one can clearly see the initial stage of the reflection process. Second, the form of the very first oscillation in the train of sinusoids within the reflected pulse depends on the phase of the reflection coefficient. The positive phase (typically $+90°$ for open-circuited or rather thick grounded electrodes on 128° $LiNbO_3$) results in a corresponding shift to the direction of inverse time by a quarter of a cycle and, consequently, the very first oscillation of the pulse appears to arrive at the receiving transducer a quarter cycle earlier than the reference signal. As discussed in the next paragraphs, with the exception of fundamental-mode 2-electrode reflectors the differences in propagation paths in the test structure used are such that they only result in phase shifts of $\pm 2\pi$, which are invisible in the total phase mismatch between the reflected signal and the reference signal.

For fundamental-mode electrodes, the width of the electrode is on the order of $\lambda_0/4$ and the center-to-center electrode separation is exactly $\lambda_0/2$. For a two-electrode fundamental-mode grating, with its center located exactly in the middle of the gap between the electrodes, the first electrode is thus shifted the distance $\lambda_0/4$ towards the transmitting transducer (port 1) and the first receiving trans-

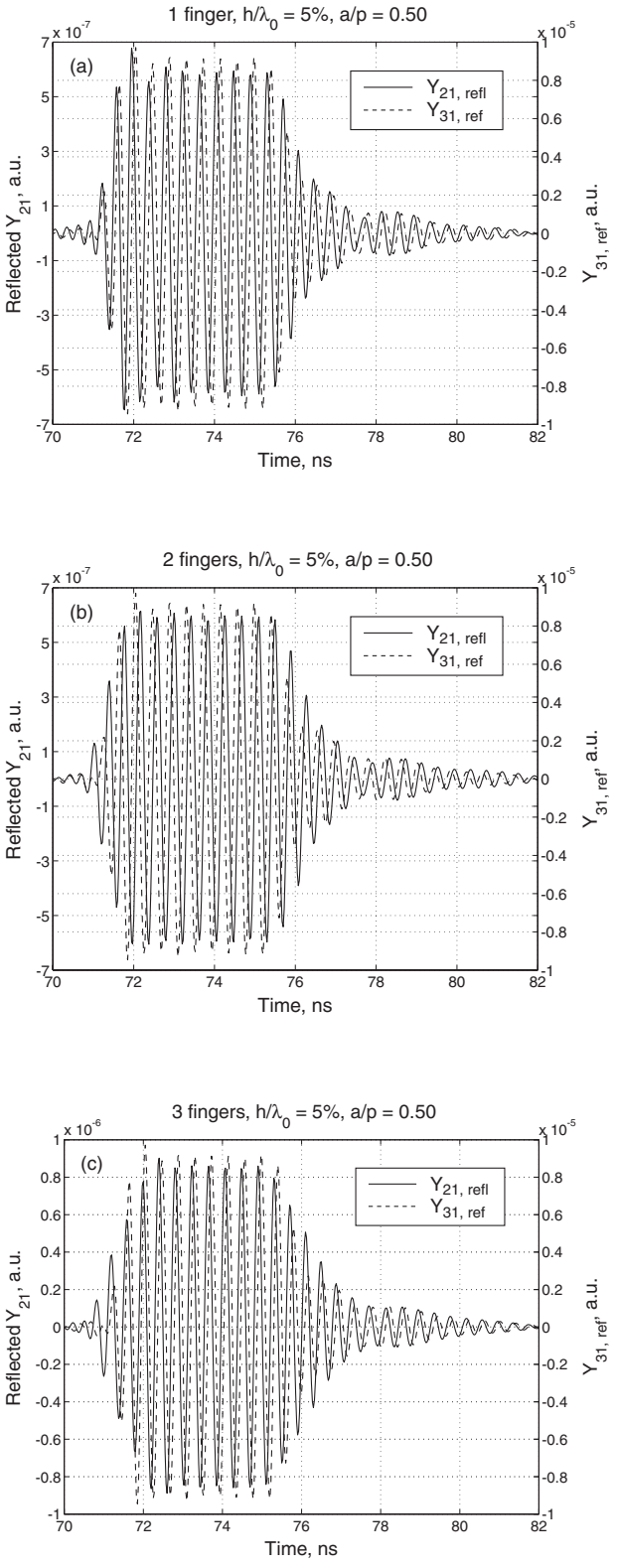

Fig. 5. Reflected pulse ($\mathrm{Re}\{Y_{21}^{r}\}$) for a fundamental-mode shorted grating ($p/\lambda_0 = 0.5$) for $h/\lambda_0 = 5\%$ and $a/p = 0.50$. (a): $N_{el} = 1$. (b): $N_{el} = 2$. (c): $N_{el} = 3$.

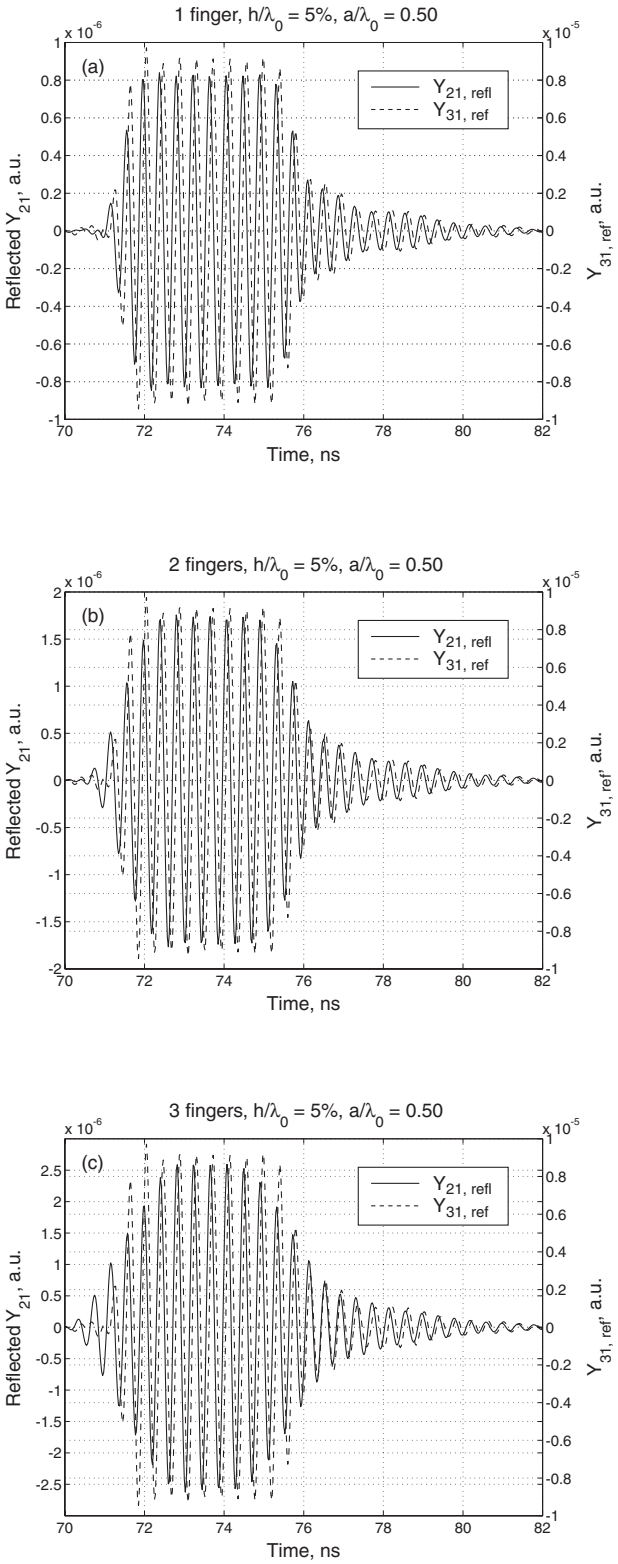

Fig. 6. Reflected pulse ($\mathrm{Re}\{\mathrm{Y}_{21}^{\mathrm{r}}\}$) for a second-harmonic shorted grating ($p/\lambda_0 = 1.0$) for $h/\lambda_0 = 5\%$ and $a/p = 0.50$. (a): $\mathrm{N_{el}} = 1$. (b): $\mathrm{N_{el}} = 2$. (c): $\mathrm{N_{el}} = 3$.

ducer (port 2). Correspondingly, the second electrode is shifted a distance exactly equal to $\lambda_0/4$ towards the second receiving transducer at port 3. As a result, the propagation path of the partial signal reflected from the first electrode is $2 \cdot \lambda_0/4 = \lambda_0/2$ shorter than the nominal propagation path with the reflection center in the middle of the reflector. This corresponds to a positive phase shift of π. Analogously, the propagation path of the partial signal reflected from the second electrode is $\lambda_0/2$ longer than the nominal propagation path. The reflected contributions thus have a difference in propagation path lengths equal to λ_0, or a full cycle, and they interfere constructively. However, when compared to the reference signal ($\mathrm{Y}_{31}^{\mathrm{d,\,ref}}$), the reflected partial signals experience an additional phase shift of $\pm\pi$ due to the difference $\pm\lambda_0/2$ in the length of the propagation path. This is visible as the total phase shift of $3\pi/2$ backward in time, which is observed as what appears like a reversed polarity of the reflected pulse in Fig. 5(b).

For 3-electrode fundamental-mode gratings, the first electrode is located at a distance exactly equal to $\lambda_0/2$ towards the transmitting and first receiving transducers, and the 3$^{\mathrm{rd}}$ electrode is located at a distance $\lambda_0/2$ towards the second receiving transducer. The different reflected contributions are again in phase and, as opposed to the fundamental-mode grating with 2 electrodes, the differences in the lengths of the propagation path with respect to the reference signal ($\mathrm{Y}_{31}^{\mathrm{d,\,ref}}$) are multiples of the wavelength. Hence, the differences in propagation path only give rise to additional phase differences equal to 2π and, as illustrated in Fig. 5(c), result in a total phase mismatch between the reference and reflected signals equal to that caused by the reflection, about $\pi/2$.

For second harmonic gratings, where the width of the electrode is on the order of $\lambda_0/2$ and the center-to-center electrode separation is exactly λ_0, the locations of the electrodes only result in additional phase differences equal to multiples of 2π. Thus, the total phase mismatch between the reference and reflected pulses is not affected by the difference in the lengths of the propagation path, see Fig. 6.

In Fig. 7, the real part of the time-domain admittance of the partial signals corresponding to reception at port 3 after direct transmission through the reflector studied ($\mathrm{Re}\{\mathrm{Y}_{31}^{\mathrm{d}}\}$) is compared to the real part of the reference signal received at port 3 (with no reflector present, $\mathrm{Re}\{\mathrm{Y}_{31}^{\mathrm{d,\,ref}}\}$). The metal thickness in each figure is $h/\lambda_0 = 5\%$, and the metallisation ratio is $a/p = 0.5$.

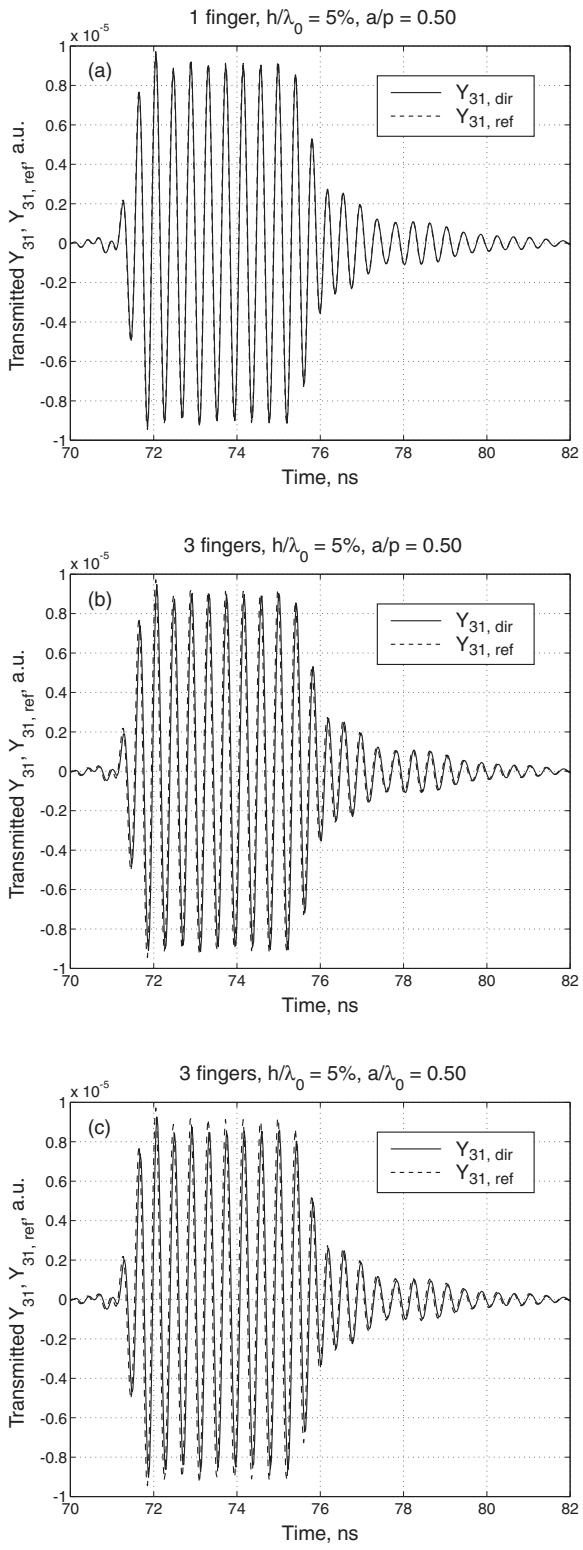

Fig. 7. Transmitted pulse ($\mathrm{Re}\{\mathrm{Y}_{31}^{\mathrm{d}}\}$) for a shorted grating for $h/\lambda_0 = 5\%$ and $a/p = 0.50$. (a): Fundamental mode ($p/\lambda_0 = 0.5$), $\mathrm{N_{el}} = 1$. (b): Fundamental mode ($p/\lambda_0 = 0.5$), $\mathrm{N_{el}} = 3$. (c): Second-harmonic mode ($p/\lambda_0 = 1.0$), $\mathrm{N_{el}} = 3$.

The conditions for the transmission differ significantly from those of reflection. The majority of the energy of the incident (= reference) signal is transmitted with minimal changes in the pulse shape. Even if multiple reflections inside the 2- or 3-electrode reflectors are taken into account, their effect on the total transmitted response will be negligible. Evidently, the only difference between the propagation paths of the reference signal and the transmitted signal is then the reflector, which interacts with the wave propagating through. Although not studied in detail, the likely interaction mechanism is increased mass-loading on the propagation path, slowing down the wave and resulting in a corresponding decrease of phase for the transmitted signal when compared to the reference signal. Hence, the transmitted signal arrives at the receiving transducer at port 3 later than the reference signal. This is in accordance with the fact that the reflected signal having a positive phase change arrives at the receiving transducer at port 2 before the reference signal is registered at port 3. The phase delay due to transmission through a short grating is manifested in Fig. 7. As expected, the delay increases with increasing grating length.

IV. Results

The rigorous FEM/BEM simulator [6, 7] was applied to evaluate the phase changes related to the reflection from and transmission through short reflectors for Rayleigh waves on 128° YX-cut $LiNbO_3$. The reflectors are either grounded or open-circuited. The materials parameters by Kovacs *et al.* [9] were used and the aluminum electrodes were assumed rectangular and isotropic. The results are presented as a function of the metallization ratio a/p (for the 2^{nd} harmonic grating, $a/p = a/\lambda_0$) and the relative electrode thickness h/λ_0.

A. Phase change at reflection

The phase change at reflection is illustrated in the time domain in Figs. 8–10 and, for comparison, the frequency-domain values for a single-electrode reflector with $h/\lambda_0 = 5\%$ are shown in Fig. 11.

The estimates for the phase change attributed to the reflection obtained with Eqs. (9) and (10) are equivalent within the accuracy of the nunerical method. Comparing the curves corresponding to $h/\lambda_0 = 5\%$ in Figs. 8 with values roughly averaged from Fig. 11, one may verify that a very good agreement is found. The difference in values obtained from the two approaches is less than 2°. For geometries with vahishing reflectivity, see Ref. [1],

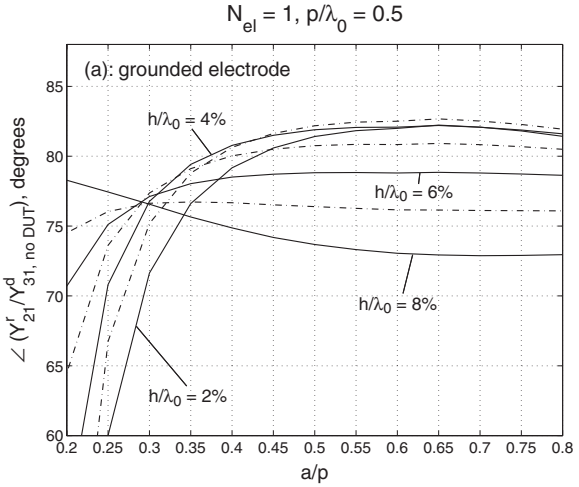

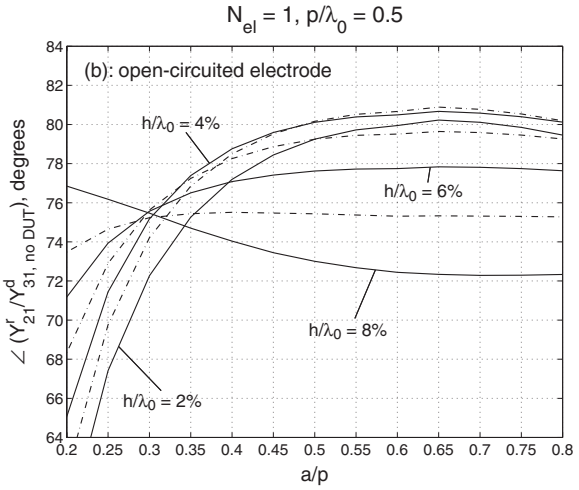

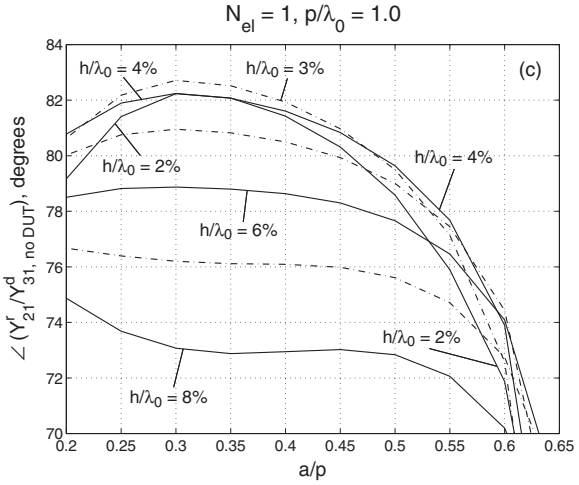

Fig. 8. Phase of the reflection coefficient from a single electrode, evaluated in the time domain, as a function of the aluminum thickness h/λ_0 and metallisation ratio a/p. (a): Fundamental mode of operation ($p = \lambda_0/2$), grounded electrodes. (b): Fundamental mode of operation ($p = \lambda_0/2$), open-circuited electrodes. (c): Second-harmonic mode ($p = \lambda_0$).

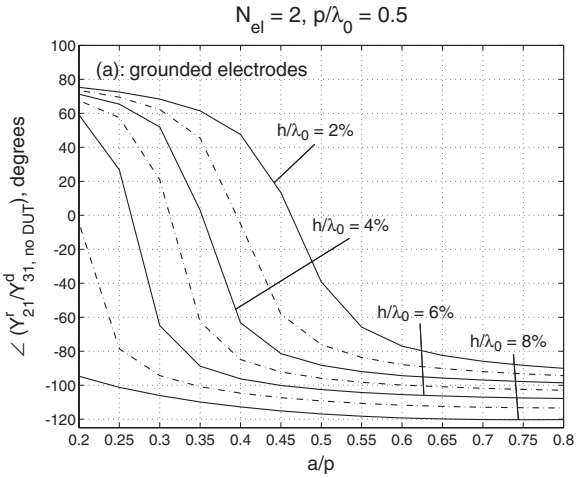

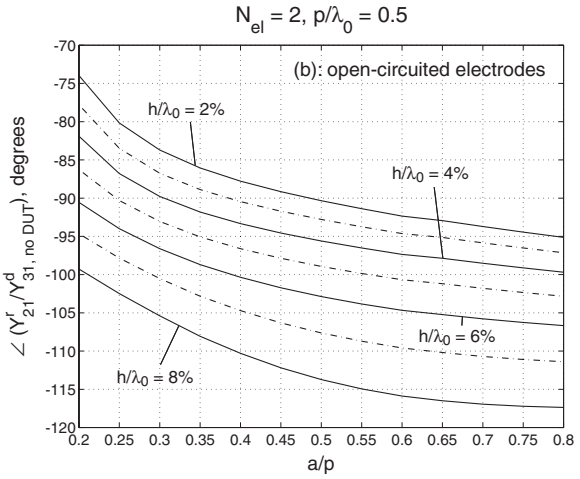

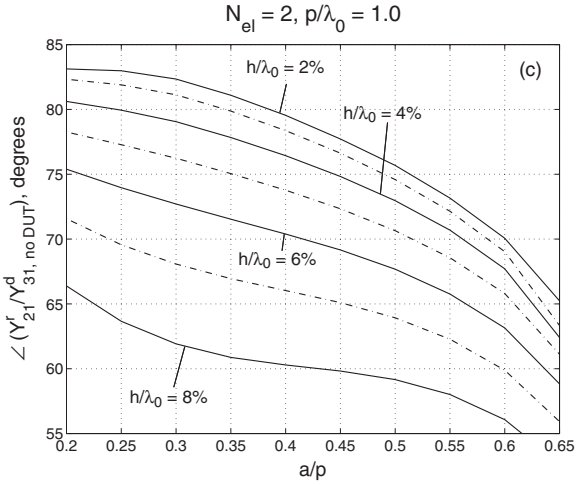

Fig. 9. Phase of the reflection coefficient from the 2-electrode grating, evaluated in the time domain, as a function of the aluminum thickness h/λ_0 and metallisation ratio a/p. (a): Fundamental mode of operation ($p = \lambda_0/2$), grounded electrodes. (b): Fundamental mode of operation ($p = \lambda_0/2$), open-circuited electrodes. (c): Second-harmonic mode ($p = \lambda_0$).

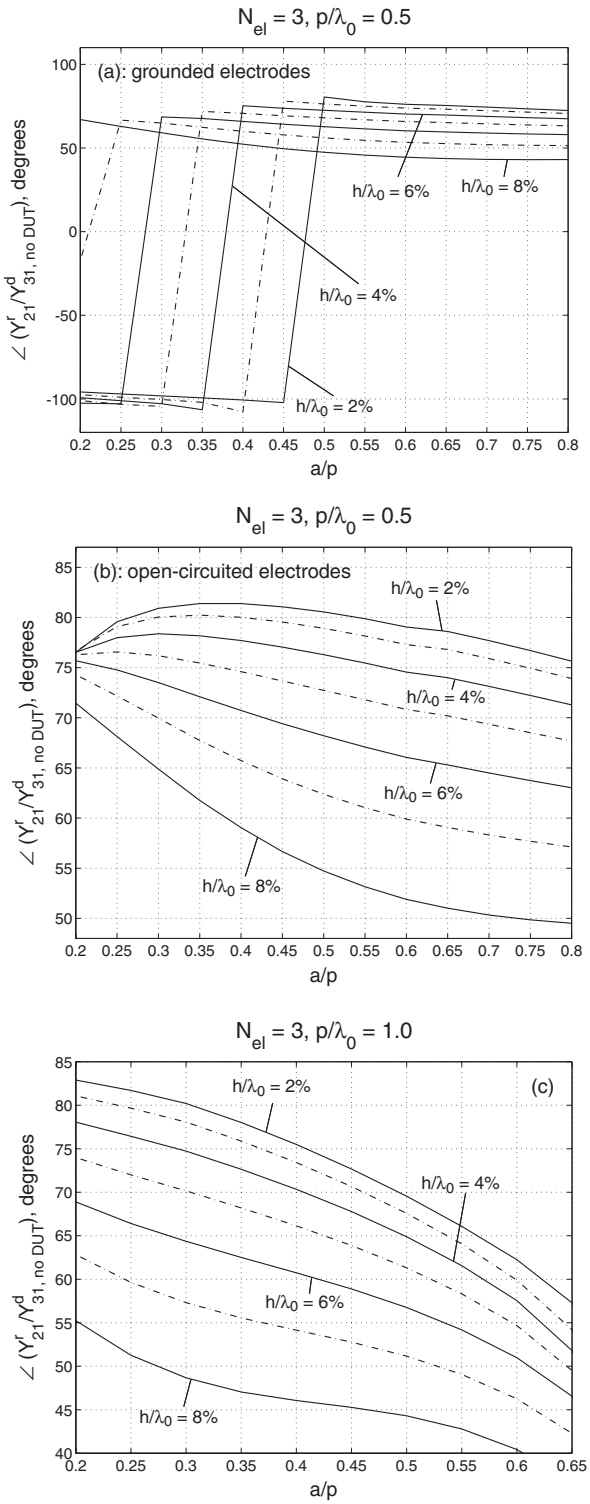

Fig. 10. Phase of the reflection coefficient from the 3-electrode grating, evaluated in the time domain, as a function of the aluminum thickness h/λ_0 and metallisation ratio a/p. (a): Fundamental mode of operation ($p = \lambda_0/2$), grounded electrodes. (b): Fundamental mode of operation ($p = \lambda_0/2$), open-circuited electrodes. (c): Second-harmonic mode ($p = \lambda_0$).

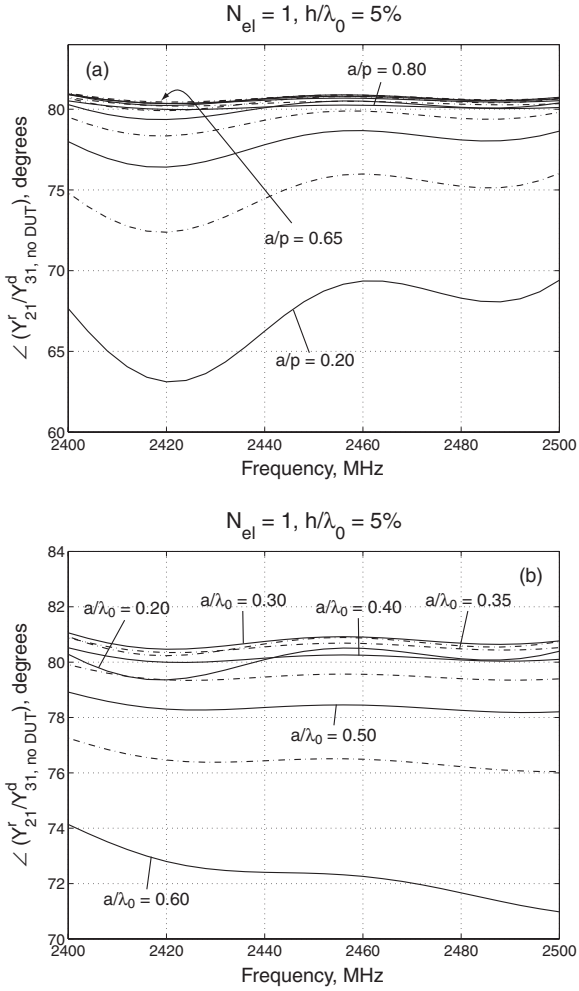

Fig. 11. Phase of the reflection coefficient from a single grounded electrode, evaluated in the frequency domain, as a function of frequency and metallisation ratio a/p. (a): Fundamental mode of operation ($p = \lambda_0/2$). (b): Second-harmonic mode ($p = \lambda_0$). Here, $h/\lambda_0 = 5\%$.

the phase of the reflection coefficient changes sign, see, *e.g.*, Fig. 9(a). In the frequency domain, a weak reflectivity implies that the spectral contributions distant from the center frequency have a relatively more significant impact on the overall reflectivity. Then, estimation of the phase using the averaging band Δf results in values of lesser accuracy.

Our results suggest that for single-electrode configurations, the phase of the reflection coefficient is relatively insensitive to the metallisation ratio for the practically interesting electrode geometries, see Fig. 8. In particular, for electrodes with thicknesses $h/\lambda_0 = 5$–7% and widths in the range $a = 0.4p_0 \ldots 1.0p_0$, the phase appears almost invariant. When combined with the strong variance in the magnitude of reflectivity, this is a very attrac-

tive feature for SAW tag applications. For two- and three-electrode configurations, for all but few individual geometries the phase change attributed to a reflection from the grating decreases with increasing metallisation ratio. The abrupt jumps crossing the lines in Fig. 10(a) are attributed to the definition range of the phase, $[-\pi, \pi]$.

B. Phase change at transmission

The phase change attributed to the transmission through a grating is illustrated in time domain in Figs. 12–14. Since, for a short grating, the absolute majority of the signal power is transmitted, the effect of multiply reflected partial signals is negligible. Consequently, the difference observed in the time-domain and frequency-domain values (the latter not shown) is practically nonexistent.

For all the cases studied, the phase delay increases with increasing metallisation ratio and electrode thickness. In the open-circuited gratings, the phase delay is slightly smaller than that in the grounded reflectors. In contrast to the phase characteristics obtained with the simple model in Sec. I, the transmission delay for single-electrode reflectors is not strictly linearly proportional to the electrode width. Moreover, it is interesting to note that, according to the simulations, there are combinations of electrode thickness and metallisation ratio for which the phase delay attributed to the transmission through the grating is equal for the fundamental and second-harmonic modes of operation (*e.g.*, grounded gratings with $N_{el} = 3$, $a/p = 0.6$ and $h/\lambda_0 = 8\%$, see Fig. 14).

V. Discussion

We have numerically studied the phase changes related to a reflection from and a transmission through a short grating on 128° $LiNbO_3$. Our quantitative results suggest that the phase change attributed to the reflection depends on both the relative electrode thickness and the metallisation ratio. Thus, for proper design of SAW devices incorporating several reflectors in the same acoustical channel, employing the nominally $\lambda_0/4$- and $\lambda_0/2$-wide electrodes studied, a tight control of phase characteristics is necessary. However, for single electrodes, according to our simulations, a combination of varying magnitude of reflectivity with invariant phase can be found for practical electrode thicknesses and metallisation ratios.

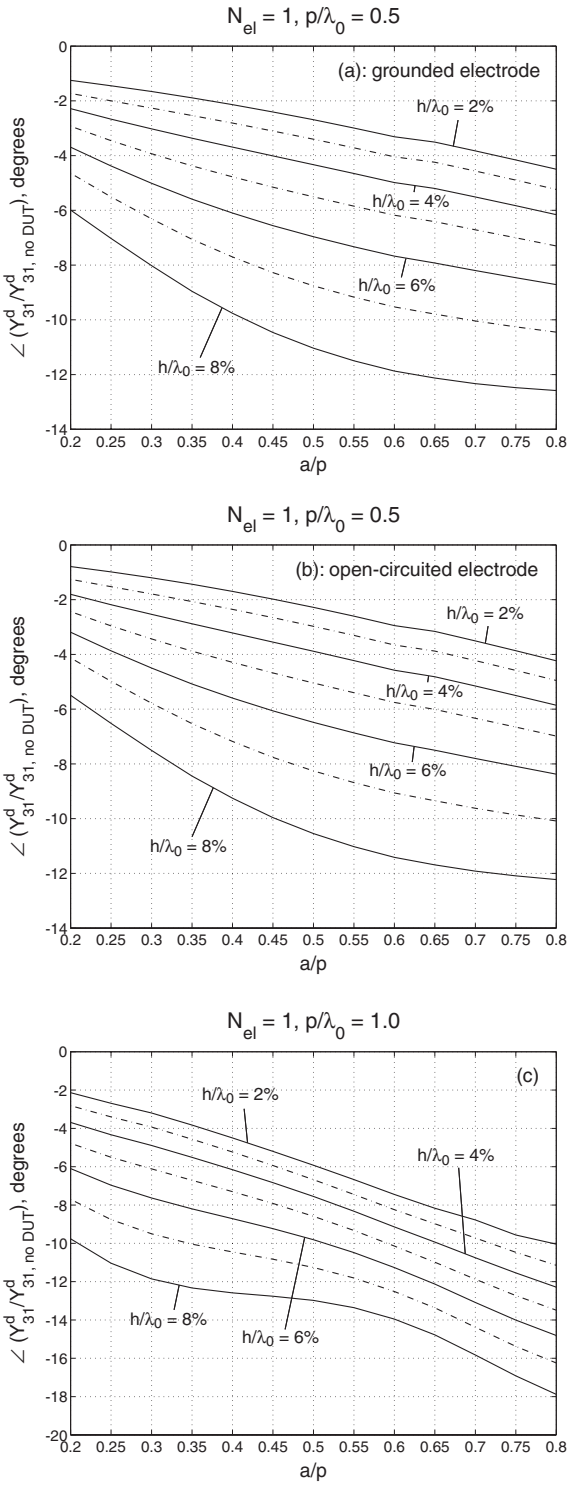

Fig. 12. Phase change attributed to transmission through a single electrode, evaluated in the time domain, as a function of the aluminum thickness h/λ_0 and metallisation ratio a/p. (a): Fundamental mode of operation ($p = \lambda_0/2$), grounded electrodes. (b): Fundamental mode of operation ($p = \lambda_0/2$), open-circuited electrodes. (c): Second-harmonic mode ($p = \lambda_0$).

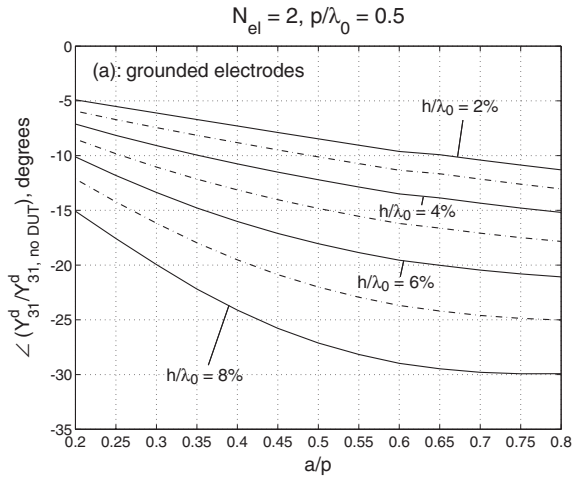

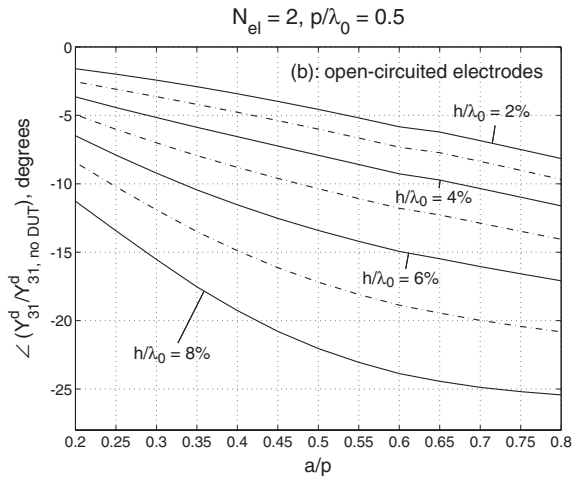

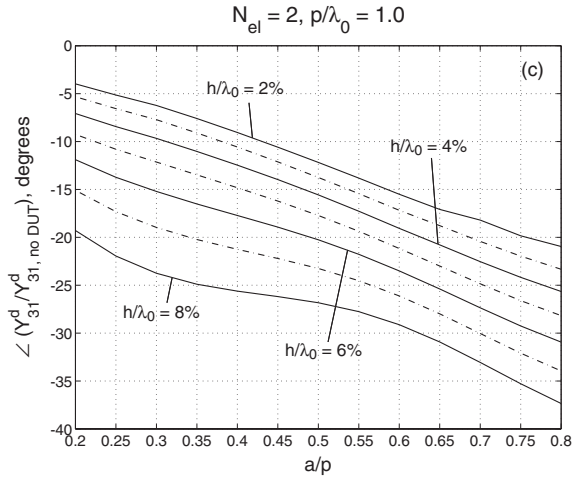

Fig. 13. Phase change attributed to transmission through a 2-electrode grating, evaluated in the time domain, as a function of the aluminum thickness h/λ_0 and metallisation ratio a/p. (a): Fundamental mode of operation ($p = \lambda_0/2$), grounded electrodes. (b): Fundamental mode of operation ($p = \lambda_0/2$), open-circuited electrodes. (c): Second-harmonic mode ($p = \lambda_0$).

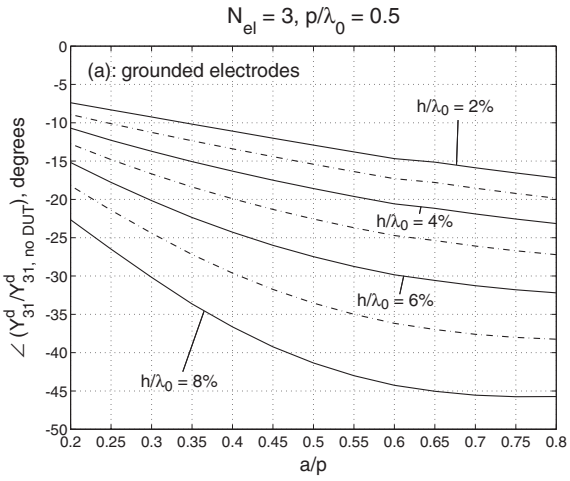

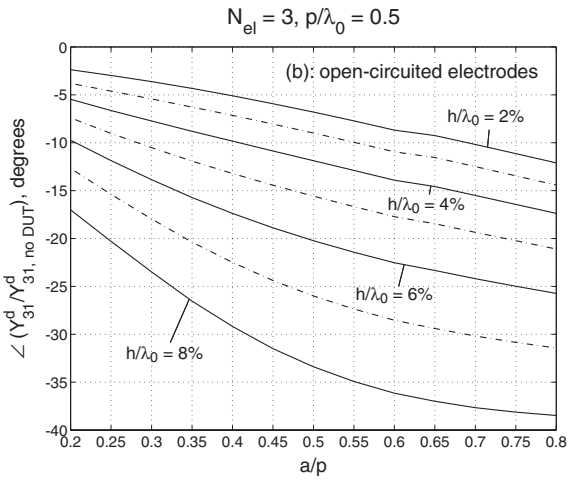

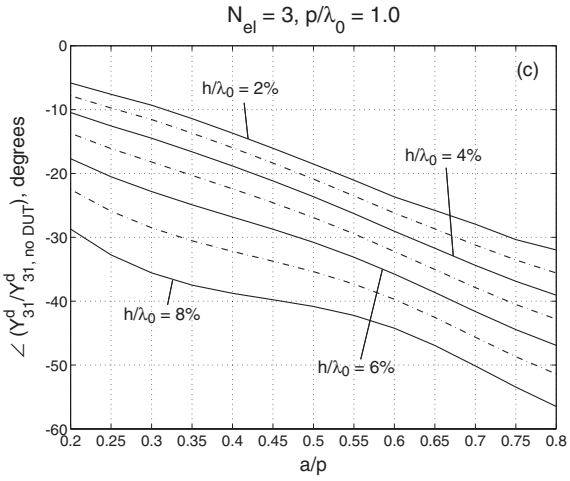

Fig. 14. Phase change attributed to transmission through a 3-electrode grating, evaluated in the time domain, as a function of the aluminum thickness h/λ_0 and metallisation ratio a/p. (a): Fundamental mode of operation ($p = \lambda_0/2$), grounded electrodes. (b): Fundamental mode of operation ($p = \lambda_0/2$), open-circuited electrodes. (c): Second-harmonic mode ($p = \lambda_0$).

Acknowledgments

The authors are grateful to Clinton Hartmann for enlightening discussions and William Steichen at Temex Microsonics SA for conferring TRANSD[1] at the disposal of HUT for this study. The first author further acknowledges the Academy of Finland for support within the Graduate School in Technical Physics and the Foundation of Technology (Finland) for a scholarship.

References

[1] S. Lehtonen, V. P. Plessky, and M. M. Salomaa, "Short reflectors operating at the fundamental and second harmonics on 128° $LiNbO_3$," *IEEE Trans. Ultrason., Ferroelectr., Freq. Contr.* **51**, No. 3, March 2004, pp. 343–351.

[2] S. Lehtonen, V. P. Plessky, N. Béreux, and M. M. Salomaa, "Minimum-loss short reflectors on 128° $LiNbO_3$,", *IEEE Trans. Ultrason., Ferroelectr., Freq. Contr.* (in print).

[3] D. P. Morgan, p. 377 in *Surface-wave devices for signal processing*, Elsevier, London, 1985, 432 pp.

[4] K. Hashimoto, pp. 26–27 in *Surface acoustic wave devices in telecommunications*, Springer, Berlin, 2000, 330 pp.

[5] M. Takeuchi and K. Yamanouchi, "New types of SAW reflectors and resonators consisting of reflecting elements with positive and negative reflection coefficients," *IEEE Trans. Ultrason., Ferroelect., Freq. Contr.* **33**, No. 4, July 1986, pp. 369–374.

[6] J. Ribbe, "On the coupling of integral equations and finite elements / Fourier modes for the simulation of piezoelectric surface acoustic wave components," PhD Thesis, CMAP / Ecole Polytechnique, 2002.

[7] P. Ventura, J.-M. Hodé, M. Solal, J. Desbois, and J. Ribbe, "Numerical methods for SAW propagation characterization," *Proc. 1998 IEEE Ultrasonics Symp.*, pp. 175–186.

[8] P. Wright, "Modeling and experimental measurements of the reflection properties of of SAW metallic gratings," *Proc. 1984 IEEE Ultrasonics Symp.*, pp. 54–63.

[9] G. Kovacs, M. Anhorn, H. E. Engan, G. Visintini, and C. C. W. Ruppel, "Improved material constants for $LiNbO_3$ and $LiTaO_3$," *Proc. 1990 IEEE Ultrasonics Symposium*, pp. 435–438.

[1] TRANSD is a FEM/BEM-based simulator for analysis of SAWs in finite electrode structures developed by Temex Microsonics SA (Sophia-Antipolis, France) in collaboration with CMAP/Ecole Polytechnique (Paris, France).